Mon. Not. R. astr. Soc. (1983) **205**, 1009–1029

Simulations of mergers between disc–halo galaxies

John Negroponte *Department of Physics, University of California, Berkeley, CA 94720, USA*

Simon D. M. White *Astronomy Department and Space Sciences Laboratory, University of California, Berkeley, CA 94720, USA*

Received 1983 March 21; in original form 1982 November 30

Summary. We have carried out a series of more than 30 simulations of the collision and merging of pairs of similar disc–halo 'galaxies'. The initial systems in these experiments contain equal amounts of mass in a near exponential disc and in a centrally concentrated non-rotating spheroidal component. In addition we treat a fraction of the disc particles as 'gas clouds' which can undergo inelastic frictionless collisions and so simulate the dissipation of energy in the highly inhomogeneous interstellar media of real galaxies. We analyse in some detail aspects of the interaction process such as the formation of bridges and tails and the loss and transfer of mass, energy and angular momentum within the galaxy pair. We also analyse the shape and velocity structure of the resulting merger remnants and their dependence on the initial conditions of the galaxy encounter. We find that if most elliptical galaxies are remnants of single mergers between comparable systems, the initial orbits of these pairs must predominantly have had low angular momenta, and the observed galaxies must be prolate objects.

1 Introduction

The last five years have seen a considerable amount of attention focused on the problem of merging galaxies and protogalaxies. Toomre & Toomre (1972) were the first to study systematically the properties of interacting pairs of test-particle discs and to produce systems which closely resemble real interacting galaxies; their numerical method did not, however, allow a consistent calculation of the ensuing merger. White (1978, 1979) performed a number of self-consistent merger simulations employing both rotating and non-rotating spherical systems as progenitor 'galaxies'. While his remnants could fit the luminosity profiles and apparent ellipticites of elliptical galaxies, their mean rotation velocities were too large except in the case of mergers between galaxies on loosely bound, low angular momentum orbits. The simulations of Aarseth & Fall (1980) showed that such mergers are common in a cosmological setting where the angular momentum distribution of merger

remnants may be similar to that of elliptical galaxies. The problem of merging *spiral* galaxies has only very recently been addressed. If one wishes to model accurately the merger of two such galaxies, each should contain a stable centrifugally supported disc. Gerhard (1981) and Farouki & Shapiro (1982) have presented simulations of mergers between discs stabilized by massive haloes, but their work covers only a limited part of the very large parameter space available and leaves a number of interesting questions unanswered. General reviews of work on galaxy merging are given by Tremaine (1981) and White (1982).

An important ingredient in the realistic simulation of spiral galaxy mergers is a dissipative component which ideally should have the properties of the gas in these galaxies. One expects the relative velocities of merging galaxies to be highly supersonic with respect to the dominant component of the interstellar medium and consequently this component should shock and dissipate kinetic energy. In observed galaxies most of the gas is in the form of dense clouds, and since most hydrodynamic codes model a continuous medium, a new algorithm seems necessary to treat the dissipative component in spiral–spiral mergers. One aim of the present work is to develop such an algorithm and to employ it in the simulation of a representative sample of mergers between 'cloudy' disc–halo galaxies; a detailed study of the properties of the merger remnants provides considerable insight into the consequences of mergers.

We begin in Section 2 with a description of our gas cloud algorithm. Thereafter we describe the construction of a disc–halo galaxy model, give a detailed analysis of its evolution and define the initial conditions for our series of mergers. In Section 3 we discuss interaction properties during the merging process and analyse the physical properties of the merger remnants, comparing the results with observations of elliptical galaxies. The final section summarizes our main conclusions.

2 Methods and initial conditions

2.1. DESCRIPTION OF CODE

In determining the type of code to be used in the present work, flexibility was our primary requirement. The code should be able to model systems containing both dissipationless and dissipational components in varying proportions; the dissipational component is envisaged as being highly inhomogeneous and consisting of coherent gas clouds. Since such highly inhomogeneous, gaseous systems are not modelled efficiently by standard hydrodynamic algorithms or by existing finite particle codes, we have decided to set up a model which treats the 'gas' as a collection of non-overlapping spherical particles of variable radius; these undergo inelastic but frictionless collisions. Embedding this scheme within an existing direct N-body integrator produces a fully self-consistent code which is both efficient and flexible.

The gravitational force between particles is modelled by the usual 'softened' gravity:

$$\mathbf{F}_{ij} = -\frac{Gm_i m_j \mathbf{x}_{ij}}{(r_{ij}^2 + \epsilon^2)^{3/2}}$$

where particles of mass m_i and m_j are at position $\mathbf{x}_i$ and $\mathbf{x}_j$ respectively. G is the gravitational constant, $\mathbf{x}_{ij} \equiv \mathbf{x}_i - \mathbf{x}_j$, $r_{ij} \equiv |\mathbf{x}_i - \mathbf{x}_j|$, and ϵ is the softening parameter, introduced in order to avoid large forces in close encounters. The resulting equations of motion are integrated using the Ahmad–Cohen force separation scheme in a fourth order predictor–corrector algorithm developed by S. J. Aarseth (Aarseth 1972; Ahmad & Cohen 1973). In addition, a certain fraction of the particles are identified as 'clouds' and may undergo collisions with other clouds in a manner which we now describe. Each cloud is assigned a collision radius,

r_c, which may vary with its position in the system, and a collision occurs whenever another cloud comes within this distance (i.e. $|\mathbf{x}_i - \mathbf{x}_j| < r_c$). The collision involves the reversal and (in general) the reduction of the relative radial velocity of the clouds. That is,

$$v_r' = -\sqrt{\alpha_c} v_r$$

where v_r and v_r' are the relative radial velocities of the clouds before and after the collision, and α_c is a parameter expressing the elasticity of the collision. Such a collision conserves momentum and angular momentum while a fraction between 0 and $1 - \alpha_c$ of the centre of mass kinetic energy is dissipated.

We choose the cloud collision radius to vary with ambient density so that the number of collisions per cloud per orbital period is roughly independent of density. This criterion may be written as

$$r_c = a n_c^{-1/3}, \tag{1}$$

where n_c is the cloud number density and the constant, a, is discussed below. This criterion ensures that the volume filling factor of the clouds is independent of local density and thus avoids the overlapping of clouds in dense regions (this was indeed our major reason for adopting equation 1). In addition to the parameters a and α_c, we found it necessary to introduce two others to ensure the efficient operation of the code in our simulations. These are a minimum relative specific energy cut-off, E_{min}, which prevents the calculation of large numbers of successive low energy collisions between clouds bound to one another, and a minimum collision radius, r_{min}, which eliminates collisions in very dense regions (where r_c is small) and so prevents a runaway increase in density.

2.2. EVOLUTION OF A DISC–HALO GALAXY

From indirect, though compelling, evidence it has become apparent that many spiral galaxies contain a massive, sub-luminous component which we shall for simplicity call the halo. The observation of flat rotation curves at large radii ($\gtrsim 20$ kpc) suggests a component whose mass increases approximately linearly with radius (Rubin, Ford & Thonnard 1980). Just such a massive spheroidal component also seems required in N-body simulations of stellar discs to ensure stability against the formation of global bar-like structures (Ostriker & Peebles 1973; Hohl, Zang & Miller 1979; Efstathiou, Lake & Negroponte 1982). However, both observation and simulation provide only lower limits to the mass and extent of the halo component; as a conservative assumption we therefore adopt a spherical and non-rotating halo of mass and radius equal to that of the disc. Note that if one wishes to identify the halo component in the models with the bulges of early-type spiral galaxies (rather than a dark component), some halo rotation would be required to fit the most recent data (Kormendy & Illingworth 1982).

We now discuss the modelling of the disc component. It is well established that the discs of spiral galaxies possess a light distribution which falls off exponentially from the centre of the galaxy (Freeman 1970). Since the mass distribution in such discs is largely unknown we simply assume it to be identical to the light distribution. To prevent the growth of small-scale clumping, a certain amount of random motion (characterized by Toomre's Q parameter) is required in the initial disc. Different numerical simulations put Q in the range 1.15–3 (Hohl 1971; Efstathiou *et al.* 1982), while observations of stellar motions in our Galaxy suggest $Q \simeq 1.5$ near the Sun, although values as high as 2 cannot be ruled out (Toomre 1974; Efstathiou *et al.* 1982). Despite its ameliorating effect on disc stability,

Q must be kept as small as possible since we want our system to model disc galaxies which have a high degree of ordered rotation. We found $Q = 1.4$ to be the minimum tolerable value. Ideally the force-softening parameter, ϵ, should be set as small as computational limitations and suppression of two-body relaxation effects will allow. Given that a major goal of the present work is to study in detail the properties of the remnants of the mergers and that we expect these to be more concentrated than their progenitors (White 1978, 1979; Gerhard 1981), we endeavoured to make ϵ a small fraction of the initial half-mass radius of our progenitor disc-halo system. Unfortunately, it rapidly became evident that a rather large value was necessary to suppress dynamical instabilities in the disc. The compromise value $\epsilon = 2$ was adopted as standard with $\epsilon = 1$ to be used for comparison test cases. $\epsilon = 2$ corresponds to $\simeq 25$ per cent of the initial disc half-mass radius, or $\simeq 40$ per cent of the disc scale length, α^{-1} (see below).

The mass fraction in H I gas in spiral galaxies varies from ~ 2 per cent in early types to ~ 10 per cent in large Sc's (Roberts 1970). In the present work we model the gas as equal mass clouds (in all $\simeq 30$ per cent of the total disc) initially distributed in position and velocity in the same way as the disc 'stars'. The cloud random velocities in our models remain similar to those of the disc particles and are a factor of $\sim 5-10$ larger than those typical of H I clouds in our galaxy (~ 10 km s^{-1}). Thus, in order to avoid unrealistic dissipation in our initial galaxy we must impose a substantial minimum relative energy, $E_{\min}$, below which cloud–cloud collisions are ignored. We chose $E_{\min} \simeq 0.2 v_t^2$ where v_t is the overall rms cloud velocity and in addition set $r_{\min} = \epsilon/2$ in order to suppress collisions when the intercloud separation becomes smaller than the force softening parameter. We set the cloud radius parameter, a (equation 1) equal to 0.5, yielding a cloud collision probability comparable to that in our own Galaxy for a cloud penetrating normal to the disc plane; this choice corresponds to a cloud mean free path of ~ 1.3 times the average intercloud separation. We assume that dissipation is efficient but leads to negligible star formation; we therefore choose $\alpha_c = 0.01$ and conserve cloud number.

Based on the considerations of the previous paragraphs we arrive at the following model. The disc component has an initial surface mass–density

$$\mu = \mu_0 e^{-\alpha r} \qquad 0 \leqslant r \leqslant R. \tag{2}$$

The disc scale-length and outer radius are related by $\alpha R = 4$. The disc particles are distributed randomly in azimuth. The halo particles are initially spherically distributed in a volume of radius R with radial density profile

$$\rho = \rho_0 / r^2 \qquad 0 \leqslant r \leqslant R. \tag{3}$$

A total of $N_g = 250$ particles of equal mass, m, are used to simulate the galaxy, $N_h = 125$ in the halo and $N_d = 125$ in the disc, a number N_c of which are treated as clouds; the standard model has $N_c = 40$. Units are chosen by setting $G = m = 1$ and $R = 20$. In such units the standard galaxy crossing time $t_c = (-2E)^{-3/2} M^{5/2} \simeq 4.5$, where E and M are the total energy and mass respectively, and its rms velocity $v_t = 3.6$. For a canonical galaxy of mass $10^{11} M_\odot$ and radius $R = 20$ kpc, the units of mass, length, time and velocity correspond, respectively, to $[m] \simeq 4 \times 10^8 M_\odot$, $[1] \simeq 1$ kpc, $[t] \simeq 10^7$ yr and $[v] \simeq 75$ km s^{-1}. The initial galaxy half-mass radius (after relaxation of halo; see below) is $R_h \simeq 7$ model units. Other parameters of our standard model are $\epsilon = 2$, $E_{\min} = 2.5$ and $r_{\min} = 1$.

Given the unstable nature of discs, we decided to evolve our halo initially in a fixed disc potential, rather than having it only approximately in equilibrium at the start of the

simulation (as in the simulations of Gerhard and Farouki & Shapiro). The halo was initially given isotropic velocities appropriate to a self-gravitating sphere with density given by (3), and was allowed to evolve with the disc component held fixed for $\simeq 6$ crossing times. In all models the halo had a smaller half-mass radius and a steeper density profile, $\rho \propto r^{-3}$, after this initial virialization. We then divided the disc into 10 annuli of equal mass, calculated the mean total radial force on each annulus and assigned each disc particle an appropriate mean rotation velocity. Radial and tangential velocity dispersions were added according to an approximate version of Toomre's local stability criterion with $Q = 1.4$, and the rotation curve was 'lowered' to account for this increased pressure support. The resulting system was within 15 per cent of being in virial equilibrium initially and its halo component showed little subsequent evolution.

Over a period of 10 crossing times our standard model galaxy appeared little different from its initial state except for a gradual thickening of the disc and cloud components. Fig. 1 shows initial and final density distributions for the various components of this model. At the final time the inner and outer parts of the halo have expanded and contracted slightly relative to one another while the halo half-mass radius has increased slightly. After ~ 9 crossing times both the disc and cloud subcomponents have expanded considerably in the outer regions, while in the inner parts the disc component has changed little but the clouds have become more compact. The shape of the profiles is still, however, close to exponential. The velocity structure of the disc also remains relatively stable. Fig. 2 shows initial and final rotation curves and velocity dispersion profiles for the disc. The particle velocities are averaged in cylindrical bins concentric with the rotation axis and the plotted points are three-point running means. This figure shows the initial rotation curve to be quite flat over the outer 90 per cent of the disc. By the end of the simulation, the inner 30 per

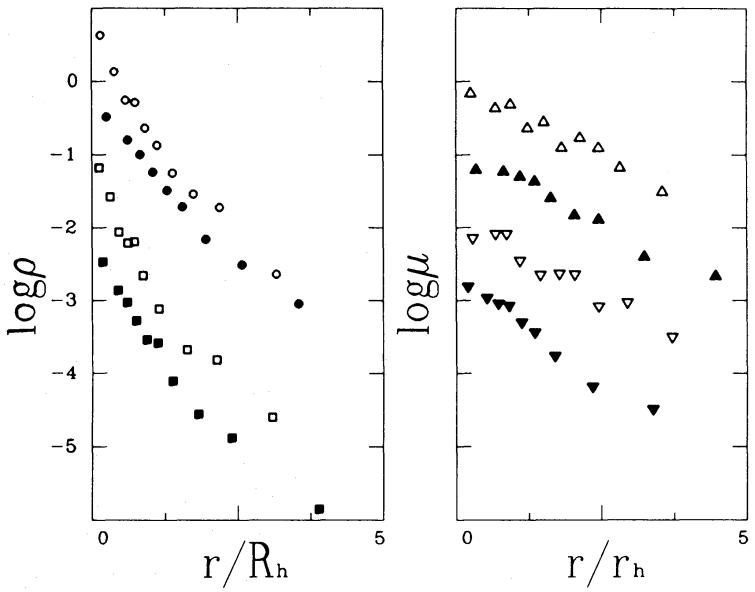

Figure 1. Mass density profiles for the standard disc–halo galaxy model. Left panel shows the volume mass density of the total (circles) and halo (squares) populations while the right panel shows the surface mass density of the disc (triangles) and cloud (inverted triangles) populations. Open and closed symbols refer to values initially and after ~9 galaxy crossing times, respectively. Points are plotted at decile mass radii normalized to the initial values of the half-mass and projected half-mass radii of the total component. The vertical scale is arbitrary and the curves have been shifted vertically with respect to each other for clarity.

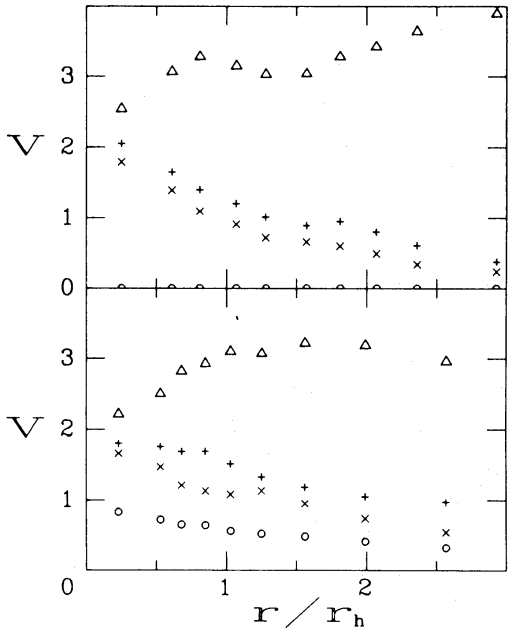

Figure 2. Rotation and velocity dispersion curves for the disc of the standard galaxy model. Velocities are calculated as described in the text. Mean rotational velocity (triangles), radial (vertical crosses), tangential (diagonal crosses), and vertical (circles) velocity dispersions are plotted as a function of projected radius normalized to the total projected half-mass radius, r_h. Upper and lower panels refer to initial and final times, respectively.

cent of the disc mass has a substantially lower mean rotation velocity than it did initially, while the rest of the disc has a flat rotation curve with a slightly lower maximum value. The final radial and tangential velocity dispersions have a somewhat flatter profile than initially with a higher mean value. The larger increase in these dispersions in the outer parts of the disc is seen as an increase in the effective Q as a function of radius in other simulations (Hohl *et al.* 1979; Efstathiou *et al.* 1982). The velocity dispersion normal to the disc plane, σ_z, increases to ~1/3–1/2 of the radial dispersion σ_r, and accounts for 3 per cent of the total final disc kinetic energy. This increase in σ_z is a result of two-body gravitational encounters and provides some idea of the effects of two-body relaxation in our merger simulations; one expects such effects to be larger in flat systems than in ellipsoidal systems such as our merger remnants. The cloud particles, in addition to gravitational two-body encounters, may also suffer highly deflective cloud–cloud collisions. In our standard model we find the z-dispersion of the clouds to be up to ~20 per cent higher than that of the disc particles. In a model with elastic collisions the cloud dispersion is consistently ~40 per cent higher than that of the disc particles.

Ideally one would prefer a standard model with a smaller softening parameter than that used here but we found such models to undergo considerable evolution. Models with $\epsilon = 1$ developed a clumpy distribution which often evolved into a bar. These models developed a thicker disc than the $\epsilon = 2$ models, their z-dispersion grew ~3 times faster, the central regions of their discs became more compact and their clouds suffered more collisional energy loss. Experiments with these and other variations of model parameters showed that both care and uncomfortable compromises are required to construct relatively stable galaxy models for use in merger simulations. Our standard model has a smaller softening and a lower halo mass than that of Gerhard, but has comparable stability. It has a larger softening and a more careful initial set-up than the standard galaxy of Farouki & Shapiro but has

half as many particles as their largest model. Table 1 of these latter authors shows the presence of strong bar-like structure when their standard galaxy is evolved in isolation.

2.3 MERGER INITIAL CONDITIONS

Assuming our initial galaxies to be axisymmetric, we require two parameters in order to specify the orientation of each at the start of a merger simulation. We adopt the representation of Farouki & Shapiro (1982). The first parameter is the angle, θ, between a galaxy's spin angular momentum and its orbital angular momentum (which we take to be in the z-direction). The second is the angle, ϕ, from the projection on the orbital plane of the spin angular momentum to the line joining the centre of the galaxies at pericentre measured in the direction of the orbit. (Notice that ϕ differs by $\pi/2$ and sometimes by a sign from the node to pericentre angle, ω, used by Toomre & Toomre 1972. Note also that the disc orientations adopted by Gerhard 1981 refer to initial values rather than the more physically relevant orientations at pericentre.) In addition to these four geometric parameters (two angles per disc), two dynamical ones are required to specify the initial two-body orbit of the galaxies. We take these to be the relative separation at pericentre, r_p, and the orbital eccentricity, e, of the initial two-body orbit. Except for the kinematic survey of Toomre & Toomre (1972) this six-parameter space has been only sparsely sampled. Gerhard (1981) has simulated elliptical, parabolic and hyperbolic collisions, but with a very limited sample of disc orientations and a single (high) pericentric distance, while Farouki & Shapiro (1982) have performed simulations for a comprehensive sample of disc orientations at a single (once again, high) pericentric distance. The aim of the present work is to cover as large a range of disc inclinations and pericentric distances as is economically feasible. In addition, we include several comparison cases in which the azimuthal angle, ϕ, and orbital eccentricity, e, are varied. Although the majority of our simulations utilized the 'standard galaxy' described in the previous section, five other initial galaxy models were also used in order to assess the effects of cloud properties and of the softening parameter on the merging process and the merger remnants. A total of more than 30 merger simulations were run in four pericentre groups ($r_p/R_h = 0.3, 0.75, 1.5, 2.2$) each containing between 5 and 9 models which differed in orientation angles or in the parameters of the progenitor galaxy model. (Standard values were changed to various combinations of the following: softening parameter, $\epsilon = 1$, number of clouds, $N_c = 0$, collision elasticity parameter, $\alpha_c = 1$, total particle number per galaxy $N_g = 500$.)

The progenitor galaxies were started at a centre-to-centre separation of 4 initial disc radii (where tidal effects are <5 per cent of the self-gravity of each galaxy), except for two elliptical encounters where the initial separation was 3 disc radii. They were then given velocities appropriate to point masses on a two-body orbit of specified energy. For parabolic mergers this energy is, of course, zero and for two hyperbolic encounters it was chosen so that the relative velocity of the galaxies at infinity would be equal to their initial internal velocity dispersion. The resulting orbital energy is about 20 per cent of the total energy of the system. The two elliptical encounters were started with an equal, but negative, orbital energy.

3 Results

In this section we discuss the main results gleaned from our series of merger simulations. We begin by describing the interaction properties of merging galaxies, in particular their morphology, interaction strength, and mass, energy and angular momentum exchange. We

then discuss the properties of the resultant merger remnants – shape, density profiles and kinematic properties.

3.1 INTERACTION PROPERTIES

Subsequent simulations have not significantly improved on the kinematic survey of Toomre & Toomre (1972) in regard to the morphology of tidally interacting disc galaxies. White (1978, 1979) and Villumsen (1982) considered only spheroidal systems while Gerhard (1981) found it difficult to reproduce the thin and well-defined 'bridges and tails' found by the Toomres. His problem, inherent in the present study also, is that self-gravitating discs are difficult to stabilize against non-axisymmetric disturbances without the introduction of substantial random velocities. As a result, the disc structure at pericentre has far less regularity than the cold discs of evenly spaced particles used by Toomre & Toomre. In particular, mergers employing a small softening parameter ($\epsilon = 1$) result in broader tidal features than mergers which use standard galaxies because of the larger random velocities in these cases. Despite these shortcomings, there are still some useful conclusions to be drawn.

First, as found by Toomre & Toomre, the prominence of the tidal tails thrown out at pericentre is a strong function of disc orientation. More nearly corotating discs result in stronger tidal tails as do discs with $\phi \simeq 90°$ or $270°$ (which corresponds to alignment of the pericentre vector and the line of nodes). By the time it reaches apocentre the disc component of a corotating galaxy has generally formed a distinct and massive tidal tail containing up to one quarter of the disc mass and consisting mainly of those particles which were furthest from the collision partner at pericentre. In addition, a number of disc particles from the side nearest the collision partner are either captured by it, or form a diffuse and transient bridge of particles connecting the two galaxy cores. As the system evolves the tail breaks up, typically into a few clumps, and continues to move outwards, some particles becoming unbound and escape; the bridge dissolves as its particles condense on to each core. Fig. 3 shows the evolution of the halo and disc components in a parabolic encounter between almost completely corotating and counter-rotating galaxies ($r_p/R_h = 1.5$, $\theta_1 = 10°$, $\theta_2 = 170°$). The disc component of the corotator clearly displays the tail and bridge evolution described above, whereas the halo component experiences a severe but diffuse tidal response. Note that by the final time a large number of disc and halo particles have been captured by the companion galaxy. In contrast, the halo and disc components of the counter-rotator are only weakly affected by the interaction with little debris and virtually no particles lost by capture. This is typical of galaxies with some degree of counter-rotation ($\theta \gtrsim \pi/2$). Galaxies which are inclined to the orbital plane but with some corotation show tidal tails in the disc component which are similar in shape to those of the corotator discussed above but which extend out of the orbital plane (see the 1000-body example illustrated in fig. 5 of White 1982). In the few cases where a good comparison is possible, the directions and shapes of these tails are similar to those seen in the kinematical study of Toomre & Toomre (1972). In some cases a pronounced tidal budge (elongated along the line joining the galaxies) can be seen just after pericentre. The cloud particles mimic the stellar disc structure except in encounters where there is sufficient overlap of the discs ($r_p/R_h \leqslant 0.75$) to cause a substantial number of collisions between clouds from different galaxies; hereafter we shall term these 'inter-galaxy' cloud collisions.

We attempted to produce a fully self-consistent model for a specific interacting system considered by Toomre & Toomre (1972): NGC 4038/9 ('The Antennae'). Our model has the disc inclinations and pericentric distance used in their work but has $\omega = -6°$ (*cf.* their

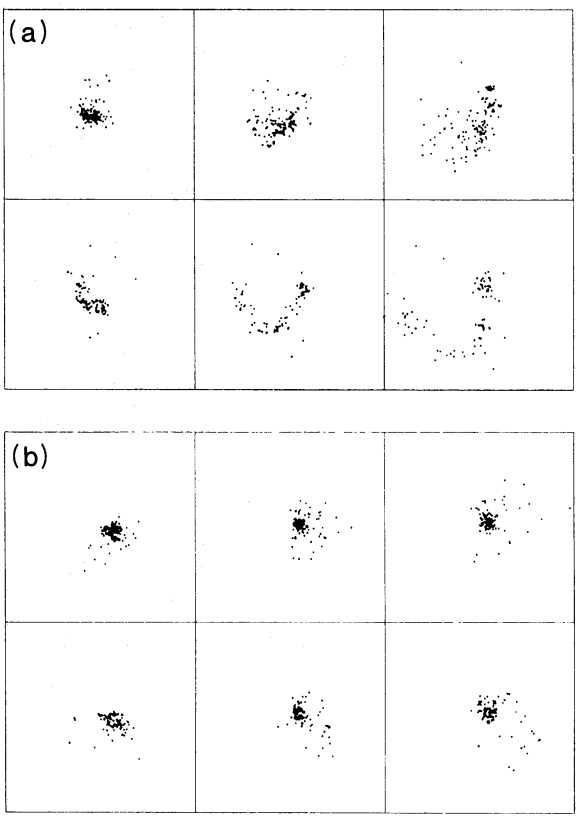

Figure 3. Snapshots of a parabolic encounter between almost completely corotating and counter-rotating galaxies. (a) halo (upper panels) and disc (lower panels) particles of the corotator are shown one, two and three single galaxy crossing times after closest approach. (b) same as (a) for the counter-rotator.

value $\omega = -30°$) and a parabolic initial orbit (*cf.* their eccentricity $e = 0.5$); the interaction between our 'active' galaxies soaks up an appreciable fraction of the initial orbital energy and the relative orbit after the first encounter is similar to that in the Toomres' calculation. One simulation of this system employed 500 particles per galaxy (250 halo, 170 disc, 80 clouds) and a plot of the particle positions corresponding to fig. 23 of Toomre & Toomre (1972) may be found in fig. 4 of White (1982). While the structure in this figure is evidently less smooth than that seen in the kinematic simulations it is certainly not a poor representation of the real system.

It is clear that the interaction strength in galaxy encounters should decrease with increasing pericentric distance and orbital energy. For rotating spherical systems White (1979) showed that the merging cross-section was also strongly dependent on the orientation of progenitor spin relative to the orbital angular momentum. Gerhard (1981) found both a similar dependence on spin direction for disc–halo galaxies and a tendency for overlapping of discs to result in more rapid merging. Farouki & Shapiro (1982) confirmed this 'overlap' effect and derived a merging cross-section for corotating discs as a function of pericentric distance and orbital energy. The present work investigates, in addition, the effect of dissipation on the merging process and the subsequent evolution of the merger remnant. The 'overlap' effect in our simulations has an additional component; a greater overlap results in a greater loss of orbital energy through inter-galaxy cloud collisions and, hence, in a faster merging time. Other trends evident in our study are that the merging time increases with increasing orbital energy, and that encounters using a dissipationless cloud component (i.e. $\alpha_c = 1$) merge at a time intermediate between their dissipational and

cloud-free counterparts. This latter effect clearly implies that cloud–cloud collisions are at least as effective at randomizing orbital kinetic energy as are tidal or violent relaxation processes.

We have attempted to obtain some quantitative results for the exchange of mass, energy and angular momentum between tidally interacting galaxies. We considered only those encounters where the two systems separated to more than 5 initial galaxy half-mass radii after their first close passage. At maximum separation we divided (albeit somewhat artifically) the system into four disjoint parts: the two cores (self-bound sub-groups), a loosely bound envelope (particles bound to the entire system, but either bound to neither core individually or almost equally bound to both) and escapers (particles with positive total energy). The details of our separation procedure may be found elsewhere (Negroponte 1982). To avoid confusion, throughout the remainder of this section we shall distinguish carefully between these 'morphological' components, 'population' components (halo, disc, cloud) and 'vector' components of the angular momentum.

Consider the question of mass exchange. In Fig. 4 we show the numbers of particles captured *from* a galaxy as a function of its inclination. The amount of mass captured varies from 0–25 per cent of the total and clearly depends both on galaxy inclination and on pair separation at pericentre. The more nearly corotating a galaxy the larger the mass captured from it by its partner. It is interesting that although the disc component typically loses twice as much material as the halo, in instances where there is significant mass transfer

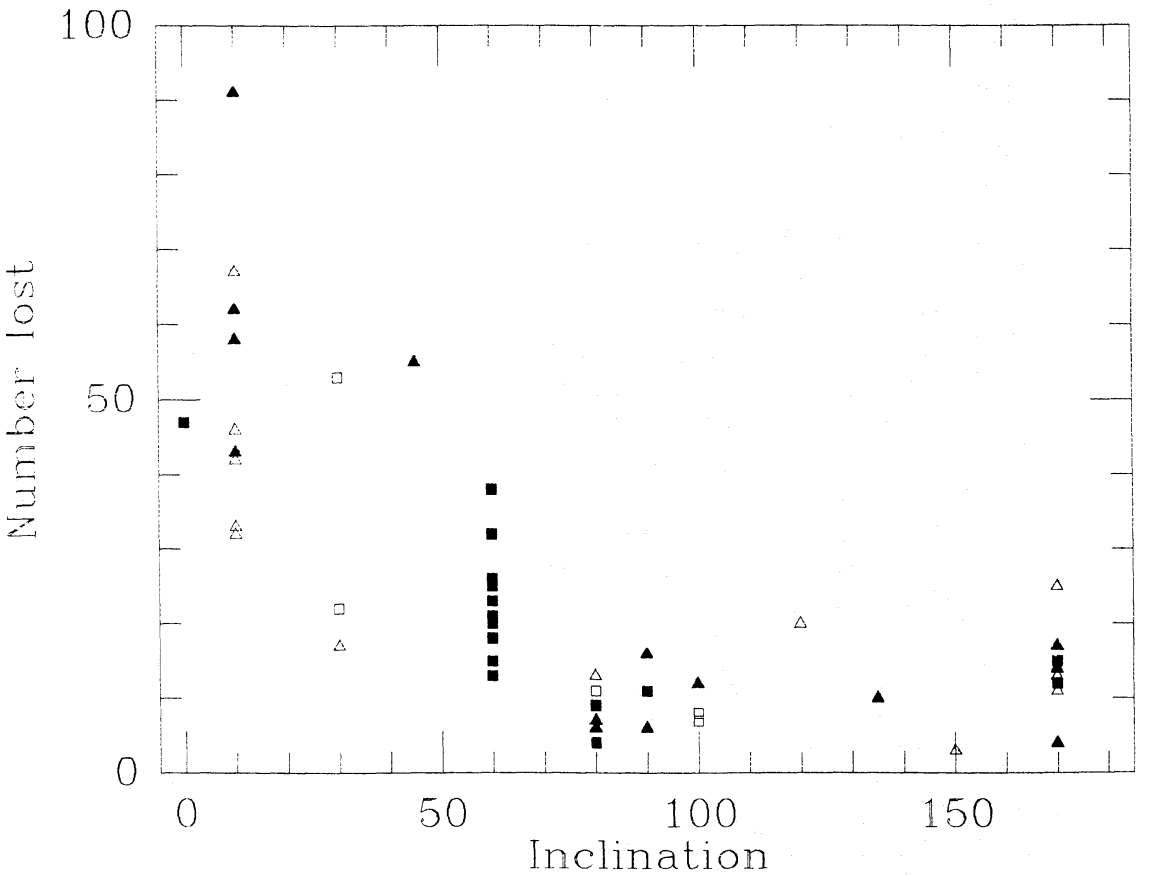

Figure 4. Particle transfer resulting from the tidal encounter of similar disc–halo galaxies. Plotted are the total number of particles captured from a galaxy by its partner as a function of its inclination (in degrees) with respect to the orbital plane. The different symbols refer to different pericentre encounters: $r_p/R_h = 0.3$ (open triangles); 0.75 (open squares); 1.5 (closed triangles); and 2.3 (closed squares).

the halo loss can also be asymmetric; an example of this is seen clearly in Fig. 3. The asymmetry may be due to direct gravitational coupling between the disc and halo components, any nett loss of disc mass instigating a similar loss of halo particles. Mass transfer (and any asymmetry therein) appears to be more pronounced for high pericentre encounters; comparing encounters between discs of similar inclination at pericentric distances of $0.3\,R_h$ and $1.5\,R_h$ we see a 30–100 per cent increase in captured mass. In addition we find that higher orbital energy results in diminished transfer. Similar results for the dependence of mass transfer on pericentric distance were found by Gerhard (1981).

The number of particles which are ejected into the loosely bound envelope or which become entirely unbound as a result of the tidal interaction may be up to 20 per cent of the initial galaxy mass. Typically this mass loss is equally shared between the envelope and escapers; it depends on the initial disc orientation and the population component considered in a similar way to the mass loss by capture discussed above. The escapers produced by the first encounter of two galaxies constitute most of the unbound mass at the end of the merging process. The latter can be up to $\simeq 11$ per cent of the total depending on the population component in question. (The maximum halo mass loss is about half of this.) In general, cloud component losses mirror those of the corresponding collisionless disc particles. The losses of other components appear essentially independent of cloud properties (the clouds constitute a small fraction by mass of the total system) whereas there is some indication that there are greater cloud losses in simulations with elastic collisions. Losses from all components seem to be independent of the choice of softening parameter.

We now consider the redistribution of energy in close encounters. Energy gain or loss may occur through two main processes, even in the absence of dissipative cloud collisions. The first is particle exchange; the binding energy of the new membership of the galaxy will differ from that of the original galaxy because of loss of former members and capture of non-members. The second mechanism is tidal heating; orbital kinetic energy may be channelled into the random motion of particles which remain within their parent galaxy. For a number of encounters we calculated the energy gained by each galaxy core, by the loosely bound envelope, and by escapers, as well as the energy lost from the orbit of the cores; all quantities were evaluated at apocentre. The total orbital energy loss in these encounters varies from 0.4 to 0.7 times the internal energy of an initial galaxy. For mergers without a dissipational component this orbital energy is expended about equally in heating the cores of the initial galaxies (and/or their exchanged particles) and in ejecting particles into the envelope or beyond. The inclusion of a collisional but *non-dissipative* component leads to somewhat more efficient conversion of orbital kinetic energy into random motions. Dissipational models employing our standard galaxy resemble models with purely stellar discs in the behaviour of their outer regions, but the energy deposited in their cores by tidal heating is largely dissipated again by cloud–cloud collisions.

We have looked at the question of angular momentum redistribution by tidal interactions in some detail. In the following discussion the angular momentum of a population component is always calculated in the rest-frame of its galaxy. The total angular momentum of captured particles is usually less than 5 per cent (and is at most ~15 per cent) that of the initial galaxy. The nett captured angular momentum almost always has a positive vector component in the direction of the orbital angular momentum, suggesting a capture configuration wherein the captured particles lag behind the captor's core. The angular momentum per particle captured is on average the same for the halo and disc components; however, the tendency to capture more disc than halo particles results in the captured disc angular momentum being larger than that of the halo. After a tidal encounter, the spin

angular momentum of the remaining galaxy core is always very different from that of the initial galaxy. First, it is greatly reduced (by up to a factor of 3) by the loss of disc particles which either are transferred or become unbound. Secondly, it is changed by tidal torques. In order to investigate these torques we have calculated the change in angular momentum of those disc and halo particles which remain in their original core after collision. We find that for disc particles the angular momentum often changes by ~50 per cent; for low inclination (i.e. nearly corotating or nearly counter-rotating) initial discs the change is roughly antiparallel to the original disc spin. The halo always gains angular momentum parallel to the orbital momentum. The change in the disc angular momentum can be understood as a response to two distinct torques. The first acts on the tidal bulge raised in each galaxy by its companion. In co- and counter-rotators the bulges in the disc component respectively lead and lag the perturber, resulting in a change in angular momentum opposing the disc spin. The second torque depends on the inclination of the disc and results from tidal compression towards the orbital plane. This torque is always along the line of intersection of the disc and orbital planes and thus depends on magnitude on the inclination angle θ and in direction on the other orientation angle ϕ.

We have determined the angular momentum carried off by positive energy escapers in our merger simulations. In the most extreme case, a merger between a corotator and a counter-rotator at an intermediate pericentric distance ($r_p/R_h \simeq 1.5$), the corotator's disc particles carry away ~70 per cent of the initial *total* angular momentum of the disc, corresponding to ~110 per cent of its spin. One expects the halo component's mass and angular momentum loss to be independent of disc properties and thus to be a function of pericentric distance and orbital energy alone. By and large, this is true but, as noted above, there does appear to be some correlation with disc losses. The maximum angular momentum loss for the halo population is 15 per cent.

3.2 REMNANT PROPERTIES

All the simulations described in the previous section were run until the merging process was complete, leaving a single remnant system. This section is devoted to a detailed discussion of the structure and dynamical properties of merger remnants. We begin by discussing remnant shapes and pattern speeds, we move on to a description of local density and velocity structure, and we close with a comparison with the observed properties of bright elliptical galaxies. In order to reduce statistical noise, all remnants in the present work are superpositions of six snapshots spanning the last three remnant crossing times of our calculations; they have been constructed separately for each of the four population components (total, halo, disc and cloud). Extreme care must be taken to ensure that no coherently varying dynamical structure is erased by this superposition. In the discussion that follows properties of these 'super-remnants' are discussed except where the contrary is explicitly stated.

Our remnants are ellipsoidal systems with shapes that range from prolate, through triaxial, to oblate, with two almost round objects. It is encouraging that they span the range of observed flattenings for elliptical galaxies. The shape of an ellipsoidal remnant can be characterized by the ratios of the length of the major-axis to those of the intermediate- and minor-axes. The inertia tensor seems an obvious choice for determining principal axis directions but its statistical properties are poor because of the large weight it assigns to particles far from the origin. We prefer to use the quantity

$$\hat{I}_{ij} = \int \rho \frac{x_i x_j}{|\mathbf{x}|^2} \, d^3x,$$

which weights all particles equally. The outskirts of remnants often contain non-axisymmetric structures left over from the early phases of interaction, while their central regions are affected by the artificial force softening and an overabundance of cloud particles. We have therefore used only particles lying between the radii containing 20 and 70 per cent of the mass when calculating $\hat{I}_{ij}$. This method is stable and yields results in accord with visual determinations of the principal axis directions, where such a comparison is possible. We compute the ratios of the principal axis lengths using White's (1978) rank-sum algorithm. Our results overestimate the flattening of nearly round systems because the inertia tensor finds the axes in which each individual snapshot appears most elliptical. We have used Monte Carlo simulations to estimate the resulting bias and to attempt to correct it (Negroponte 1982).

We find that in all our remnants the direction of the shortest axis is roughly normal to the orbital plane. The most evident trend relates the ratio of major and minor axes to the inclinations of the progenitor discs. With only a few exceptions, lower inclination discs give rise to flatter remnants. This occurs because tidal stretching and tail formation are confined mainly to the orbital plane for low inclination discs, whereas inclined (and partially corotating) discs spew mass in directions out of the orbital plane and so produce rounder remnants. (While this effect is roughly three times as important for the disc as for the halo component, it is still significant for the latter, showing that the concentration of the disc and cloud components to the orbital plane is perturbing the halo.) For discs lying in the orbital plane, the minor-axis flattening is roughly independent of the direction of the disc spin. For intermediate inclinations a substantially flatter remnant results from a merger with corotating galaxy spins than from an otherwise identical initial condition with the spins reversed. For the highest inclination mergers the direction of spin has little discernible effect on flattening.

Using non-rotating spherical model galaxies as progenitors, White (1978) found a smaller range of flattenings than we see in the halo components of our remnants, once again suggesting that the highly flattened disc component is affecting the halo in remnants of low inclination encounters. White (1979) also found flatter remnants for corotating than for counter-rotating progenitors. This is because his initial systems possess no intrinsic flattening and the shape of the remnant is determined by spin orbit resonances alone. Gerhard (1981) quotes flattenings (calculated somewhat differently than ours) for two of his models which agree roughly with our results for similar models. Farouki & Shapiro (1982) give flattenings for seven oblate remnants and in all cases their results are less flat than we would predict, sometimes by a factor of ~ 2. In addition, they find an inclination dependence which is not consistent with our results. The reason for these discrepancies is not clear, but they may, in part, reflect differences in the measure of flattening used.

A second trend we find is a dependence of the ratio of the intermediate axis to the major axis on the pericentric distance of the encounter. Quite generally, mergers with $r_p/R_h \leqslant 0.75$ result in preferentially prolate or triaxial remnants while those with $r_p/R_h \geqslant 1.5$ yield oblate remnants. Prolate structures similar to the low pericentre remnants have been found in other simulations of mergers and seem to be a general feature of such encounters (White 1978, 1979; Miller & Smith 1980). These prolate remnants will be discussed further below. Mention should also be made of some suggestive trends visible at a lower level of significance than those just discussed. The major-to-minor axis ratio in our remnants appears roughly independent of pericentric distance (for fixed initial disc inclinations). In most cases the directions of the principal axes for the different population components roughly coincide and are roughly independent of radius within the remnant. In general the flattening behaviour of the cloud component differs from that

of the other components; but this difference is far from systematic. One reason for this may be the fact that strong dissipation has resulted in a large fraction of the clouds occupying a small central region not much larger than the softening length. Another is undoubtedly statistical noise resulting from the small number of particles involved. Finally, there is the question of the evolution of the remnant flattening. About one quarter of the remnants were evolved for more than 10 remnant crossing times after the progenitor galaxies had merged. In the process the axial ratios in most of these remnants became systematically between 10 and 20 per cent rounder suggesting that two-body encounter effects are beginning to become important over such evolution times.

In describing the motion of the remnant principal axis directions relative to some inertial frame, we use individual snapshots rather than the super-remnants described above, and a coordinate system with origin at the remnant centre (defined as the centre of the mass of the 20 most bound particles) and with one axis normal to the orbital plane. This axis usually points roughly along the total angular momentum vector of the remnant. For all non-spherical remnants one can determine the angle between the major axis (for triaxial or prolate remnants) or at least the major axis–intermediate axis plane (for oblate remnants) and the orbital plane. In more than 80 per cent of the remnants this angle is less than 20°; it shows no strong correlation with merger parameters other than the direction of the

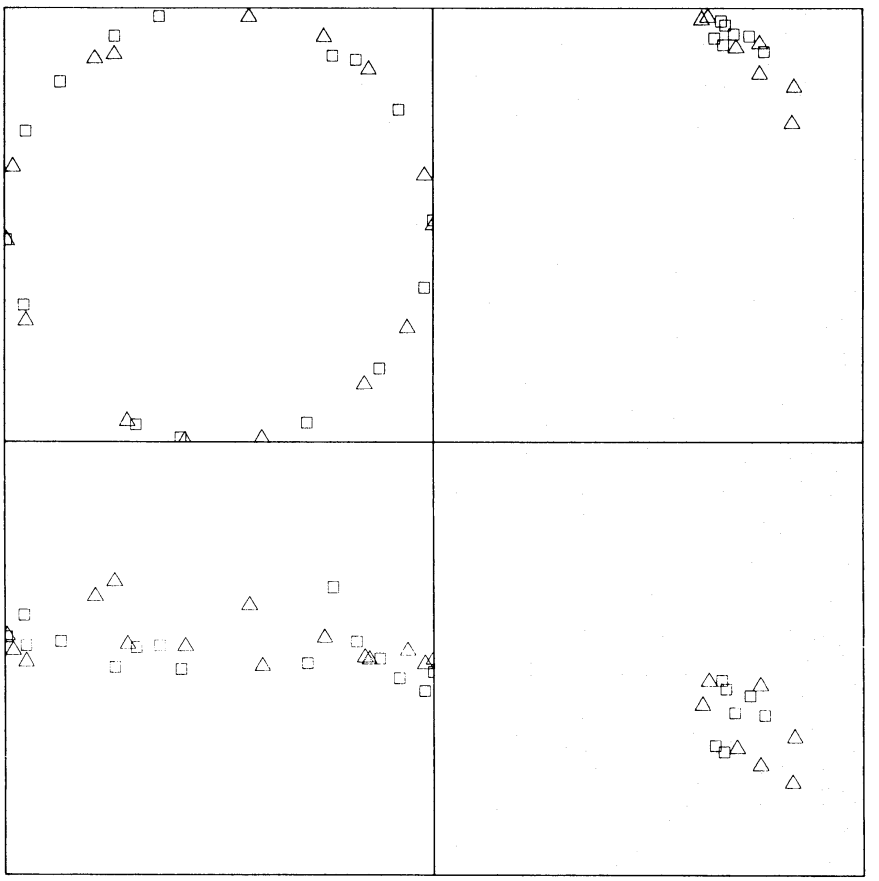

Figure 5. Remnant major axis direction as a function of time for two parabolic encounters: $r_p/R_h = 0.75$, $\theta_1 = \theta_2 = 30°$ (left panels); and $r_p/R_h = 0.3$, $\theta_1 = 10°$, $\theta_2 = 170°$ (right panels). Each point gives the unit vector from the centre of the remnant along the semi-major axis. Upper and lower panels show projections of this vector on to the orbital plane and in a plane perpendicular to the orbital plane, respectively. Squares and triangles refer to halo and disc population components.

remnant angular momentum. For prolate and triaxial remnants, the major-axis direction can be plotted as a function of time. In several cases we found it to move regularly in a circle for more than one rotation yielding a well-defined pattern speed. Other models presented almost static patterns. Fig. 5 shows plots of the motion of the major axis for two such mergers. The major axis of the first remnant (the result of a parabolic encounter at $r_p/R_h = 0.75$, $\theta_1 = \theta_2 = 30°$) rotates uniformly and always lies within 15° of the orbital plane. Its period is 15 times the crossing time of the initial galaxies or 9 times that of the remnant. It is notable that all population components move with the same pattern speed despite their diverse initial structure and dynamics. As might be expected, this prolate remnant has considerable streaming motion along the bar, a phenomenon discussed further below. In contrast, the second remnant shown (the result of an almost head-on collision with $r_p/R_h = 0.3$, $\theta_1 = 10°$, $\theta_2 = 170°$) has an almost stationary pattern in all its population components, despite the fact that the specific angular momentum of the disc particles is one-third as large and is oppositely directed to that of the halo particles. It appears that this extremely flattened, triaxial structure is primarily supported by anisotropic velocity dispersions (its axes are in the ratios 0.45 : 0.71 : 1). We find no simple relationship between pattern speed and initial total angular momentum.

Previous simulations of mergers of spherical (White 1978, 1979; Villumsen 1982) and disc–halo systems (Gerhard 1981; Farouki & Shapiro 1982) show the remnants to have smooth Hubble-law mass–density profiles ($\rho \propto r^{-3}$) over most of their mass. The wide variety of the initial systems suggests that this final profile is characteristic of the merging process itself, and results from violent relaxation during the coalescence of the two progenitor cores. The present set of numerical experiments largely confirms these findings, showing in addition that the profile is independent of remnant shape. The inclusion of a dissipational component alters somewhat the mass distribution while leaving the density profile essentially unchanged. Plots for the total mass and for each of the three population components show that in most remnants the density run of all but the cloud component is fitted well by a power law of slope –3 to –3.25, excluding the innermost point. Projected surface mass–density profiles are well fitted by a power law of slope –2 between the 20 and 70 per cent mass points; these curves are independent of the direction of projection and of remnant shape. These results agree both with those of previous studies, and with observations of bright elliptical galaxies. The relative concentration of the disc and halo populations is very model-dependent. The mean value of the ratio of half-mass radii for the disc and halo populations in a sample of 15 remnants with similar initial galaxy models is 1.17 ± 0.27. The corresponding value for the three $\epsilon = 1$ stellar remnants is 0.91 ± 0.10. Gerhard (1981) finds the disc component to be slightly more concentrated than the halo in his remnants but attributes this to the extra core mass and the more extensive halo used in his simulations. Farouki & Shapiro (1982), however, find the disc component to be much more compact than the halo in their remnants with a mean half-mass radius ratio of 0.45 for a sample of 10 systems (Farouki, private communication). The reason for this substantial discrepancy with our results is unclear. Farouki & Shapiro also obtain a value of 18 for the ratio of the radii containing 80 and 20 per cent of the bound mass in their remnants (Farouki, private communication); this is a factor of about 1.5 larger than the corresponding value found in the present work and that of White (1979), and larger still than that quoted by Gerhard. The discrepancy here may reflect differences in the softening parameters used (see below). The mean density of the inner 20 per cent of our remnants is higher than that of the progenitors by factors between 1.2 and 3.5. This spread is much larger than that found by Farouki & Shapiro and the high values we obtain are attributable to the dissipation of energy in the cloud component.

The cloud component is, in general, much more compact in our remnants than the other components, its inner 30 per cent having essentially constant density and its outer 70 per cent following the power law of the other components. This high degree of concentration is entirely due to energy loss in dissipative cloud–cloud collisions. Mergers in which the collisions were elastic resulted in the remnant's cloud component behaving in essentially the same way as the stellar component. The presence of this compact component in mergers with dissipation brings about a contraction of the half-mass radii of halo and disc components by 15–20 per cent but the shape of their density profiles is scarcely altered. The fact that the cloud component occupies a small region in the core of our remnants and often has 40 per cent of its mass inside the softening radius makes detailed study of its dynamics uninteresting observationally and suspect from a theoretical point of view. For this reason it is discussed only indirectly in the remainder of this section. While information on the structure of the gaseous subsystem in a merger remnant is clearly of greater interest, our rather crude code can only tell us that dissipation brings most of the gas into the central regions. Observations of NGC 7252 by Schweizer (1982) suggest that it may form a nuclear disc there, but our code has too few particles and too little resolution to allow us to study this. We find that there is a clear dependence of the mass distribution on the softening parameter, especially in remnants with a dissipational cloud component. Although the power-law shape of the profile is not much altered, a more 'core–halo'-like distribution develops in simulations with $\epsilon = 1$ with the 20 and 80 per cent mass radii moving inwards and outwards by ~25 per cent. The half-mass radius is, however, more or less unchanged.

While the density structure of a remnant is constrained mainly by conservation of mass

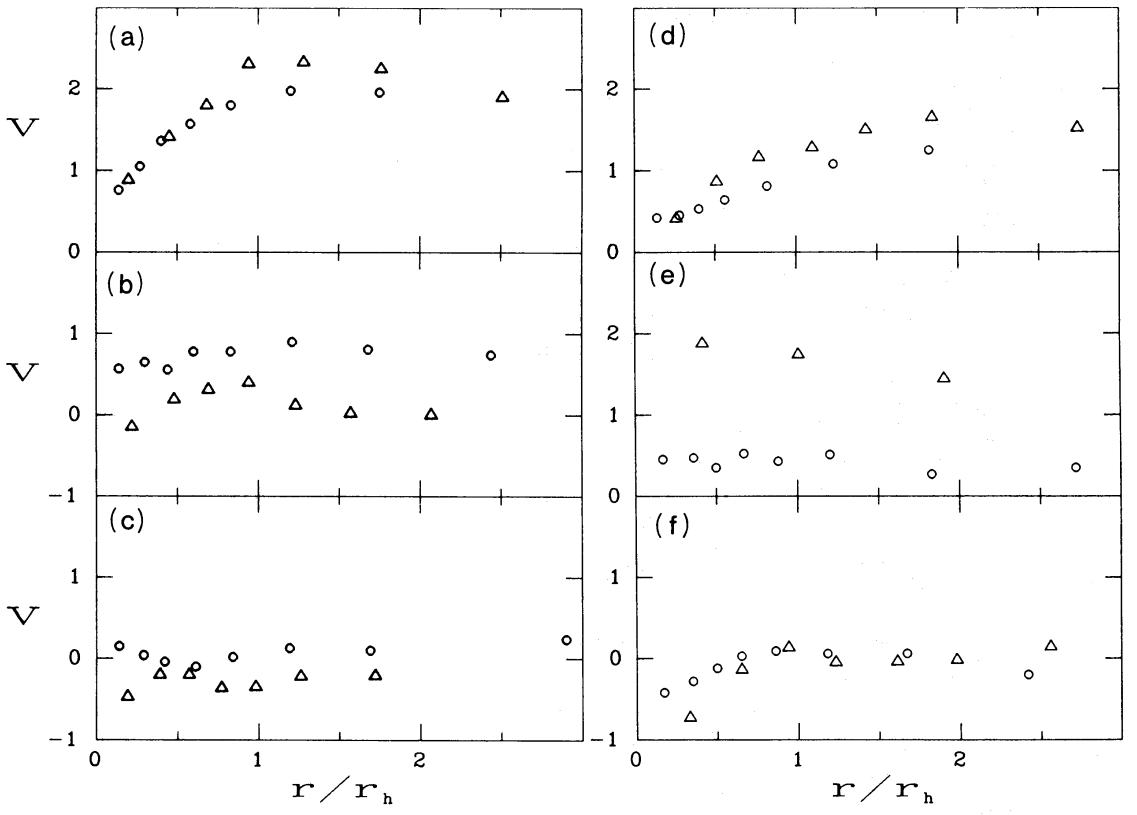

Figure 6. Projected rotation curves for selected remnants described in the text. (a)–(c) show mean rotation velocity for three different remnants projected along the intermediate axis; (d)–(f) show the rotation curves for a single remnant projected onto its three principal planes. Circles and triangles refer to the total and disc populations, respectively.

and energy, its velocity structure is in addition dependent on its total angular momentum, and so should be a function of the orbital angular momentum and the spin orientations of the progenitor galaxies. We have calculated rotation curves by projecting our remnants on to various planes and averaging particle velocities in strips parallel to the apparent minor-axis. The principal axes and apparent flattenings for these projected remnants are determined using two-dimensional analogues of the methods described above. In addition, only particles with projected position vectors lying within 30° of the apparent major axis are used in the rotation curve determination. This restriction attempts to model narrow slit spectral observations; it results in an increase of the apparent rotation velocity by up to 30 per cent in the inner regions, showing that apparent rotation velocities tend to be highest along the apparent major axis. Escapers are included in these calculations but outlying points are often not plotted in the diagrams discussed below.

Fig. 6(a)–(c) show rotation velocities for three remnants seen in projection along their intermediate axes. These result from two high pericentre encounters ($r_p/R_h = 2.2$; $\theta_1 = \theta_2 = 60°$ and $\theta_1 = \theta_2 = 170°$) and from a low pericentre merger of almost co- and counter-rotating galaxies ($r_p/R_h = 0.3$; $\theta_1 = 10°$, $\theta_2 = 170°$), respectively. While (a) is typical of the rotation curves we find and is essentially flat, (b) and (c) have interesting additional features. First, their relative maxima conform to expectations based on the progenitor disc inclinations (see also Gerhard 1981; Farouki & Shapiro 1982). It appears that the inner half of (b)'s disc component shows rotation in the orbital sense, whereas the outer parts possess little or no rotation. The disc component of this remnant lost less than 10 per cent of its initially small (6 per cent) share of the total angular momentum to escapers. Presumably the outer parts of each progenitor disc primarily populate the outer regions of the remnant explaining the low resultant velocity there (*cf.* White 1980; Gerhard 1981). In merger (c) 8 per cent of the corotators' disc particles carry away 50 per cent of this progenitor disc's total angular momentum. Not surprisingly the inner 70 per cent of the remnant's disc particles show nett counter-rotation. The effect is small, however, and one would certainly not expect it to occur in a similar encounter at a higher pericentric distance (*cf.* Gerhard's model PB).

Several of our low pericentre prolate–triaxial remnants have large streaming velocities parallel to their major axis (up to 20 per cent higher than along the intermediate-axis). Rotation curves for a remnant of a low pericentre ($r_p/R_h = 0.75$) encounter between similarly inclined partial corotators ($\theta_1 = \theta_2 = 30°$) are shown in Fig. 6(d)–(f) for projections along the intermediate, major and minor axes. This is the remnant whose systematic pattern rotation is illustrated in Fig. 5. The large streaming velocity in the disc component of this remnant explains how it can have twice as much angular momentum as the halo component but still present the same pattern speed. The velocity dispersion in our remnants is roughly constant out to the half-mass radius and then falls gradually, sometimes decreasing by up to a factor of 3 in the outer regions. This behaviour was found also by Gerhard (1981) and Farouki & Shapiro (1982). In addition, the dispersion can be highly anisotropic; for example, in the non-rotating triaxial remnant of Fig. 5 there is little streaming motion and the mean-square velocities inside the half-mass radius are in the ratio 1.3 : 2.5 : 2.9 along the minor, intermediate and major axes respectively. Similar results were found by White (1979), Villumsen (1982) and Gerhard (1981), and are discussed in more detail by Farouki & Shapiro (1982).

To the maximum apparent rotation velocity, V_m, and the velocity dispersion, σ, one can add the apparent flattening or ellipticity ($\epsilon = 1 - b/a$) of the remnant as a third observable quantity. It is well known that V_m/σ as a function of ϵ is a simple, but extremely useful, indicator of global dynamics. Binney (1978) has calculated theoretical curves in

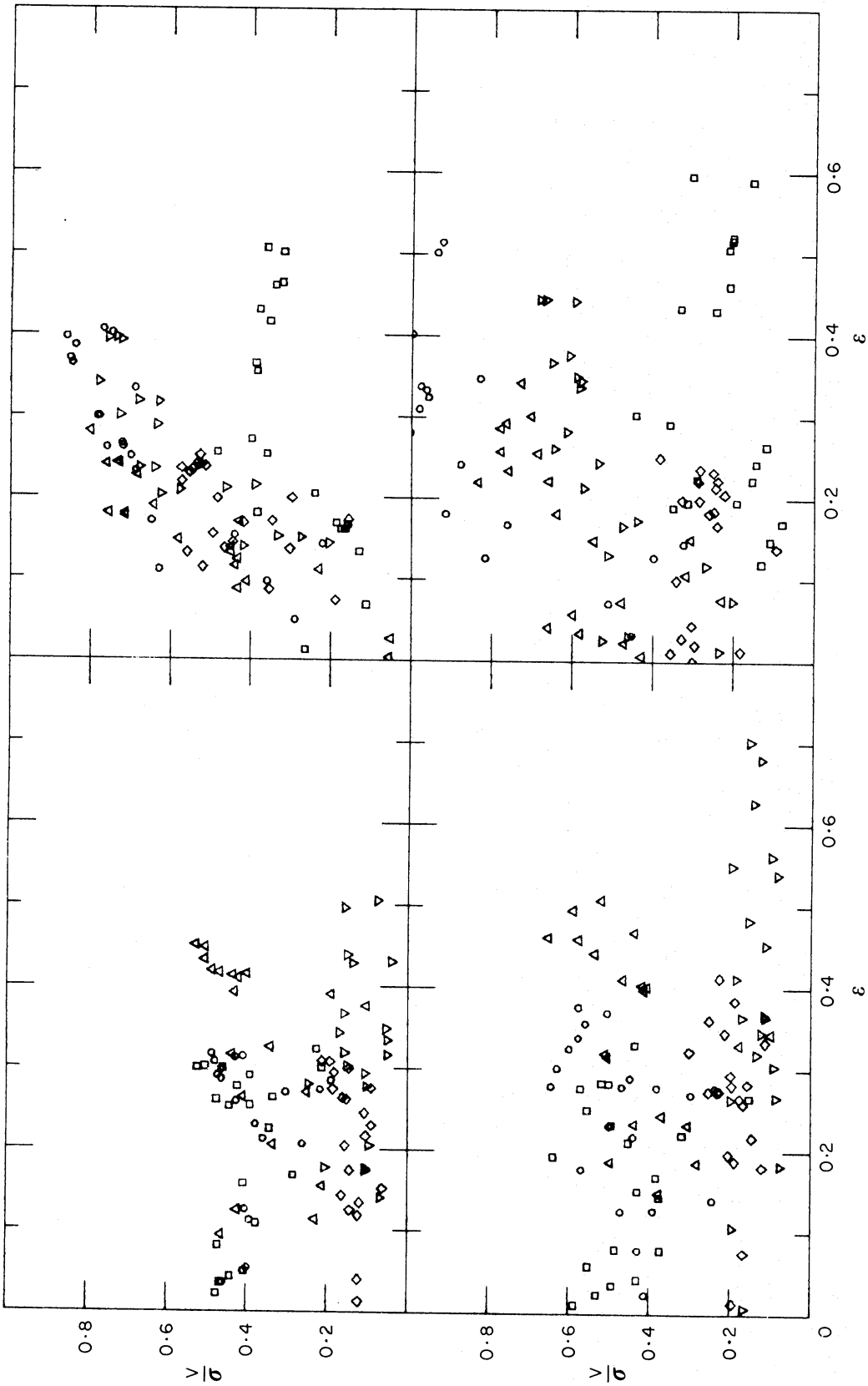

Figure 7. Maximum velocity of the apparent major axis rotation curve normalized by the line-of-sight dispersion of the inner half of the mass is plotted as a function of ellipticity for projections of various merger remnants. The two left-hand panels show results for low pericentre mergers; the two right-hand panels show similar results for high pericentre mergers. In each pair of diagrams the upper panel gives results when all particles are treated equally and the lower panel shows what would be seen if only the disc particles were visible.

the $V_m/\sigma - \epsilon$ plane for ellipsoids with varying degrees of rotational support and pressure anisotropy, while the number of observations of these quantities in elliptical galaxies is steadily increasing (Bertola & Capaccioli 1975; Illingworth 1977; Schechter & Gunn 1979; Efstathiou, Ellis & Carter 1980; Davies 1981). The surprisingly low rotation velocities found have led to a resurgence of interest in the structure of elliptical galaxies and to reconsideration of the merger hypothesis for their formation (Toomre 1977; Tremaine 1981; White 1982; Binney 1982). Several authors have calculated V_m/σ and ϵ for remnants of merger simulations (White 1979; Gerhard 1981; Farouki & Shapiro 1982). These studies must, however, be regarded as incomplete either because the progenitor galaxies did not contain a disc component (White) or had very limited parameter space coverage (Gerhard; Farouki & Shapiro). One of the major aims of the present study was to produce a $V_m/\sigma - \epsilon$ diagram for mergers between realistic progenitors with a more complete and less biased sample of disc inclinations, pericentric distances and viewing angles.

In order to separate the effects of varying pericentric distance from those of varying disc inclination, we have considered two groups of mergers, one at low pericentre distance ($r_p/R_h \leqslant 0.75$) and one at high pericentre distance ($r_p/R_h \geqslant 1.5$); each contains five simulations which use our standard initial galaxy and has a representative sample of disc inclinations. We projected each super-remnant on to 20 randomly chosen planes (corresponding to as many random viewing angles) and calculated its apparent major axis rotation curve and the apparent velocity dispersion of the inner half of its mass as described above. The apparent bias-corrected flattening and a corresponding ellipticity, ϵ, were also calculated for each projection. The $V_m/\sigma - \epsilon$ diagrams for the total and disc components of the two pericentre groups are shown in Fig. 7. The low pericentre sample has a median V_m/σ value of 0.25 if all particles are considered or of 0.37 if only initial disc particles are included. Their patchy distribution in the V_m/σ plane indicates that our rather small sample of disc inclinations is still not ideal. Notice the presence of points at small ϵ and large V_m/σ and also at large ϵ and small V_m/σ. These are prolate remnants seen end-on and down the rotation axis respectively. The higher pericentre group of remnants has a median V_m/σ value of 0.48 when all particles are considered. The disc component shows a large spread in V_m/σ values because of a strong dependence on disc inclination while the halo component (not shown here) has a correlation of V_m/σ with ϵ which resembles White's (1979) results for mergers of spherical systems and is parallel to Binney's (1978) oblate line but at lower values of V_m/σ.

It is immediately apparent from a comparison with available observational data that while our models span the observed range of ellipticities, many of them have too high a V_m/σ value. In order to fit the data one is forced to appeal to a special subset of possible merger initial conditions, namely low pericentre encounters ($r_p/R_h \lesssim 0.75$) or encounters in which disc spin angular momentum is antiparallel to the orbital angular momentum. Our estimates of V_m/σ are unlikely to have systematic errors larger than about ~20 per cent resulting from the effects of softening or the highly dissipative cloud component (as judged from a comparison of models with differing ϵ and cloud parameters). Thus while prolate remnants resulting from low pericentre mergers may be able to fit the observed V_m/σ data, the high pericentre oblate remnants have too large a variation in V_m/σ and a median value ~2.5 times too high to be acceptable. Hence, if bright elliptical galaxies are to be identified as merger remnants, our results favour the hypothesis that they are intrinsically prolate.

4 Conclusions

Our simulations of mergers between pairs of disc–halo galaxies containing a dissipative

'gaseous' component produce ellipsoidal remnants with properties similar to those of elliptical galaxies. Both the properties of the tidal interaction and the properties of the remnant depend on the initial conditions of the encounter. In particular we note the following.

(i) The orbital energy loss and the rapidity of the merger depend on the orientation of the spin angular momenta of the progenitor discs. Galaxies with disc planes only slightly inclined to the orbital plane merge faster than those with high inclinations; the physical overlap of the disc results in an enhancement of the stellar dynamical interaction and of the dissipation of orbital kinetic energy in the gaseous component. During the tidal interaction, galaxies whose spin aligns partially with the orbital angular momentum display strong characteristic morphological features (bridges and tails) in their disc population. After the tidal encounter the system is typically made up of two galaxy cores surrounded by a loosely bound envelope of particles and some escapers. Corotating galaxies lose and exchange mass, energy and angular momentum much more readily than do counter-rotating galaxies. For strongly interacting pairs, tidal effects channel a large amount of orbital energy roughly equally into internal random motions within each galaxy core, into the exchange of particles between the cores, and into creating a loosely bound envelope and unbound escapers; energy loss in a dissipative component can substantially cool the tidally heated galaxy cores. The initial spin angular momentum of a galaxy can be altered in several ways by the encounter: loss of particles can reduce the spin by $\sim 1/2$; tidal torques can reduce the remaining spin by $\sim 1/2$; and captured particles may add an amount equal to $\sim 1/5$ of the remainder (the captured angular momentum has no strongly preferred direction although it generally has a positive component along the orbital angular momentum). Mass loss and angular momentum loss occur predominantly at the first encounter of two galaxies and can be as high as 10 and 40 per cent respectively for a merger between corotating galaxies; the corresponding fractional losses for the disc population alone can be a factor of 2 larger.

(ii) All the remnants in these simulations are featureless ellipsoidal systems with principal axis ellipticities which vary between 0 and 0.7, thus spanning the range observed in elliptical galaxies. The minor axis is in all cases roughly parallel to the orbital angular momentum. The flattening is largest for low inclination initial discs, and has very little dependence on the direction of their spin; for intermediate inclinations, corotating discs produce flatter remnants than counter-rotating ones. The shape of the remnants varies in a systematic way from prolate to oblate as the pericentre distance of the encounter increases from 0.3 to 2 times the half-mass radius of the initial galaxies. Some prolate remnants have bar-like forms which rotate uniformly in the same sense as the initial orbit. All remnants have smooth Hubble law ($\rho \propto r^{-3}$) mass–density profiles over most of their mass; the dissipative cloud component becomes much more centrally concentrated than the halo or disc populations, which finish up with roughly similar distributions. We see no evidence for the cloud component settling into a new disc in any of our remnants; this is likely to be a result of the inadequacies of our method (*cf.* Schweizer's 1982 observation of NGC 7252 where such a new disc appears to have formed at the very centre of the remnant). The projected mass–density profiles of our remnants fit the observed luminosity profiles of elliptical galaxies reasonably well. Their rotation curves are in most cases flat over much of the system; the maximum rotation velocity depends mainly on the total initial angular momentum. For the halo population, the maximum rotation velocity varies monotonically with pericentre distance, whereas for each pericentre distance the maximum rotation velocity of the disc population depends on the orientation of the initial discs; it ranges between 0 and 0.9 of the corresponding value for the initial disc. The velocity dispersions are in general anisotropic, being smallest along the minor axis of the remnants. This anisotropy

is the main source of flattening in low angular momentum remnants. Some prolate remnants exhibit large streaming motions along their major axis. For a suitably selected sample of sky-projected remnants, we have calculated apparent rotation velocity maxima, line-of-sight velocity dispersions, and apparent ellipticities for comparison with observations of elliptical galaxies. In order to fit the low observed rotation velocities we need predominantly low angular momentum mergers; if ellipticals are indeed the remnants of such mergers, they must be prolate.

Acknowledgments

This work has been made possible by grants CS28-80 and C55-81 from the California Space Agency and by NSF grant AST-8114715.

References

Aarseth, S. J., 1972. In *Gravitational N-Body Problem,* ed. Lecar, M. Reidel, Dordrecht, Holland.
Aarseth, S. J. & Fall, S. M., 1980. *Astrophys. J.,* **236,** 43.
Ahmad, A. & Cohen, L., 1973. *J. Comp. Phys.,* **12,** 389.
Bertola, F. & Capaccioli, M., 1975. *Astrophys. J.,* **200,** 439.
Binney, J., 1978. *Mon. Not. R. astr. Soc.,* **183,** 501.
Binney, J., 1982. *Morph. Dyn. Gal.,* eds Martinet, L. & Mayor, M., Geneva Observatory.
Davies, R. L., 1981. *Mon. Not. R. astr. Soc.,* **194,** 879.
Efstathiou, G., Ellis, R. S. & Carter, D., 1980. *Mon. Not. R. astr. Soc.,* **193,** 931.
Efstathiou, G., Lake, G. & Negroponte, J., 1982. *Mon. Not. R. astr. Soc.,* **199,** 1069.
Farouki, R. T. & Shapiro, S. L., 1982. *Astrophys. J.,* **259,** 103.
Freeman, K. C., 1970. In *Stars and Stellar Systems,* vol. 9, (ed. Kuiper, G. P.), University of Chicago Press.
Gerhard, O. E., 1981. *Mon. Not. R. astr. Soc.,* **197,** 179.
Hohl, F., 1971. *Astrophys. J.,* **168,** 343.
Hohl, F., Zang, T. & Miller, J. B., 1979. NASA Ref. Pub., 1037.
Illingworth, G., 1977. *Astrophys. J.,* **218,** L43.
Kormendy, J. & Illingworth, G., 1982. *Astrophys. J.,* **256,** 460.
Miller, R. H. & Smith, B. F., 1980. *Astrophys. J.,* **235,** 421.
Negroponte, J., 1982. *PhD thesis,* University of California.
Ostriker, J. P. & Peebles, P. J. E., 1973. *Astrophys. J.,* **186,** 467.
Roberts, M., 1970. In *Stars and Stellar Systems,* vol. 9, ed. Kuiper, G. P., University of Chicago Press.
Rubin, V. C., Ford, W. K. & Thonnard, N., 1980. *Astrophys. J.,* **238,** 471.
Schweizer, F., 1982. *Astrophys. J.,* **252,** 255.
Schechter, P. L. & Gunn, J. E., 1979. *Astrophys. J.,* **299,** 472.
Toomre, A., 1974. In *Highlights of Astronomy,* vol. 3, ed. Contopoulos, G., Reidel, Dordrecht, Holland.
Toomre, A., 1977. *Evol. Gal. Stell. Pop.,* eds Tinsley, B. M. & Larson, R. B., Yale University Observatory.
Toomre, A. & Toomre, J., 1972. *Astrophys. J.,* **178,** 623.
Tremaine, S., 1981. In *The Structure and Evolution of Normal Galaxies,* eds Fall, S. M. & Lynden-Bell, D., Cambridge University Press.
Villumsen, J. V., 1982. *Mon. Not. R. astr. Soc.,* **199,** 493.
White, S. D. M., 1978. *Mon. Not. R. astr. Soc.,* **184,** 185.
White, S. D. M., 1979. *Mon. Not. R. astr. Soc.,* **189,** 831.
White, S. D. M., 1980. *Mon. Not. R. astr. Soc.,* **191,** 1P.
White, S. D. M., 1982. *Morph. Dyn. Gal.,* eds Martinet, L. & Mayor, M., Geneva Observatory.